Geophysical Journal International

Geophys. J. Int. (2014) **199,** 499–513
GJI Geodynamics and tectonics

doi: 10.1093/gji/ggu271

Mantle accommodation of lithospheric shortening as seen by combined surface wave and teleseismic imaging in the South Island, New Zealand

Bill Fry,[1] Donna Eberhart-Phillips[1,2] and Fred Davey[1]

[1] *GNS Science, PO Box* 30368, *Lower Hutt* 5040, *New Zealand. E-mail: b.fry@gns.cri.nz*
[2] *Department of Earth and Planetary Sciences, University of California Davis, Davis, CA* 95616, *USA*

Accepted 2014 July 14. Received 2014 June 30; in original form 2014 February 26

SUMMARY

The Pacific and Australian plates in the South Island, New Zealand (NZ) converge at a rate of about 4 cm yr^{-1}. Accommodation of the continental part of this convergence in the lithospheric mantle is both poorly understood and currently controversial yet it is a problem of fundamental importance for understanding lithospheric thickening. End-member possibilities range from the classical model of asymmetric subduction to symmetric viscous thickening. Seismic tomography has the potential to image this process. However, tomographic images to date are poorly constrained due to the lack of appropriate earthquakes. Improved teleseismic tomography of the region has been achieved by increasing data coverage and applying a novel scheme of correcting for crustal structure by ray tracing through a newly created model of shallow shear wave velocity derived from the inversion of noise-based dispersion measurements. Our resulting models suggest the lithospheric mantle high velocities at the continental plate boundary extend no deeper than approximately 125 km, evidence against both previous models of viscous drip and typical asymmetric subduction zones. This high velocity core extends from north to south along the axis of South Island suggesting that mantle convergence is accommodated along the older, mid-Cenozoic, plate boundary. West of South Island, a high velocity west dipping zone may define the remnant Cretaceous subduction zone that has been distorted by Cenozoic transcurrent deformation. We present our new 3-D seismic velocity models together with a compatible tectonic model and discuss their implications for the nature of lithospheric evolution at this convergent boundary.

Key words: Tomography; Mantle processes; Plasticity, diffusion, and creep; Continental tectonics: compressional; Dynamics of lithosphere and mantle.

1 INTRODUCTION

The Pacific–Australian Plate boundary crosses from northeast to southwest of the South Island of New Zealand (Fig. 1), where it is dominantly a transpressive continental plate boundary linking the east dipping subduction zone off southwestern South Island with the west dipping subduction off northeastern South Island and eastern North Island. South Island's existence is largely the result of the plate tectonic deformation of the region along the Pacific–Australian Plate boundary since its inception during the mid-Cenozoic. Prior to this time, the land mass of South Island was extremely low lying with only a small proportion of the present landmass above sea level (Suggate *et al.* 1978; Balance 1993). This was a result of the extension and thinning of the New Zealand microcontinent lithosphere during the late Cretaceous extension, erosion and subsidence (cooling) associated with the break-up of Gondwana and the onset of seafloor spreading between New Zealand, Australia and Antarctica. About 45 Ma the Pacific–Australian Plate boundary developed, extending from the rifted margin off southwest Campbell Plateau, through to the axis of the old Cretaceous convergent margin off east Australia (Sutherland 1999). Initially this plate margin was dominantly transtensional. It then developed mainly as a transcurrent boundary until about 5 Ma bp when a significant component of convergence commenced leading to the thickening of the lithosphere and the emergence of the South Island and Southern Alps.

The geology of the South Island is generally split into two provinces corresponding largely to the eastern margin of the Australian Plate and to the adjacent Pacific Plate crust, separated by the Alpine Fault (Fig. 2). West of the Alpine fault, Western Province rocks form basement and comprise Cambrian Takaka and Ordovician Buller metasedimentary terranes (Cooper 1979, 1989; Munker & Crawford 2000), intruded by Devonian and Cretaceous granitoids. Western Province rocks are considered to be a fragment of Gondwana continental crust (Cooper 1989). Limited sampling by

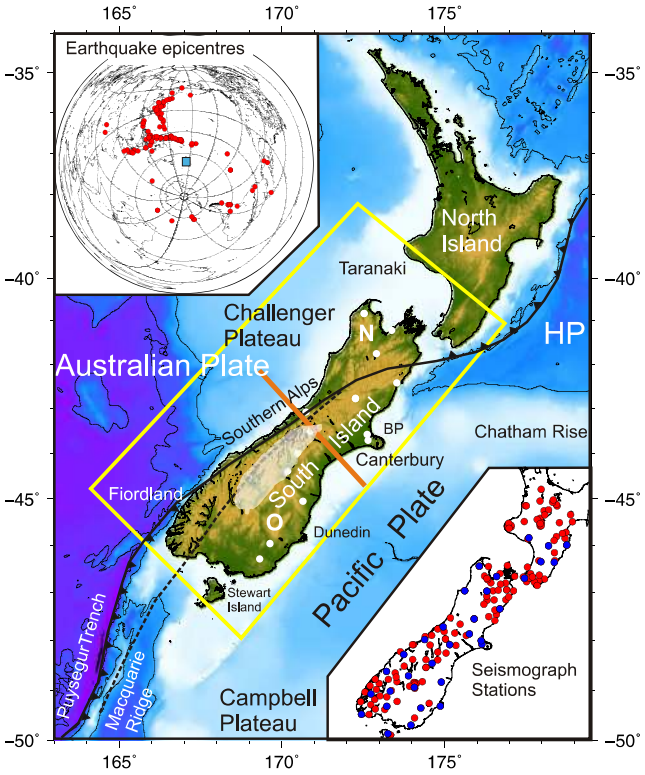

Figure 1. New Zealand region. Present plate boundary shown by solid black line with triangles marking the subducting boundary. Early Tertiary Plate boundary south of the present plate boundary shown by black dashed line. White circles are the locations of seismographs used for the receiver function analysis (Spasojevic & Clayton 2008). White transparent shading is the extent of the –50 mGal Bouguer gravity anomaly. The yellow box shows our tomographic study region and the region represented in Figs 6–9 and S5. The orange line marks the location of the profile in Fig. 3. 'N' marks the Nelson region, 'O' the Otago region, 'BP' is Banks Peninsula and 'HP' the Hikurangi Plateau. Top inset shows the epicentres (red circles) for the earthquakes used in the study, the blue square is New Zealand. Projection is equidistant azimuthal for the globe, latitudes and longitudes every 30°. Lower inset are the locations of the seismograph stations used, blue circles for the ones used in the surface wave analysis, all filled circles were used for the teleseismic tomography.

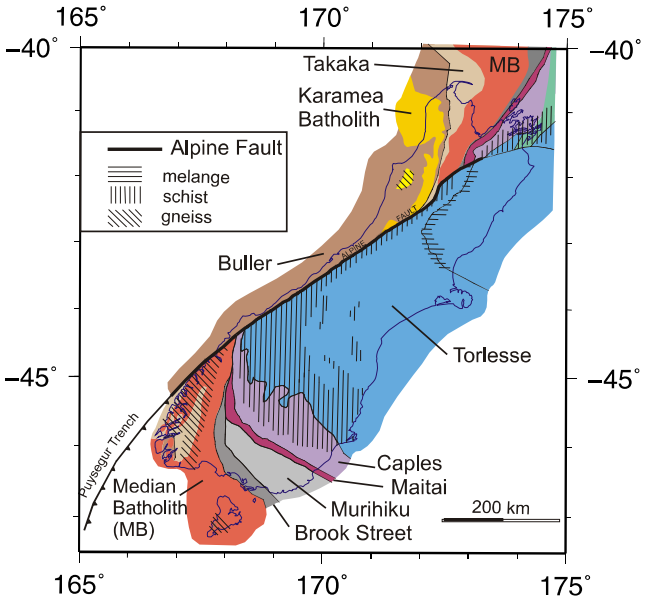

Figure 2. Simplified basement geology of the South Island, New Zealand (after Mortimer 2004). The Takaka and Buller Terranes form the Western Province that is separated from the Eastern Province (Torlesse, Caples, Maitai, Murikiku and Brook Street terranes) by the Median Batholith.

drillholes shows that similar rocks occur on the offshore Campbell and Challenger plateaus (Wodzicki 1974; Beggs *et al.* 1990; Wood 1991). Eastern Province rocks comprise a sequence of five Mesozoic island arc and metasedimentary terranes (Mortimer 2004)—Brook Street island arc terrane, Murihiku fore arc metasediments, Maitai terrane containing ophiolitic rocks of oceanic crust origin, Caples terrane of volcanogenic metasediments and the Torlesse metasediments of continental origin that have all been accreted to the Gondwana crust. The latter two terranes are partially metamorphosed to schist grade.

The structure and development of the South Island orogen and the adjacent region during the transpressive phase is of interest as the central part is considered to be a young, relatively simple, continental convergent plate boundary. As such, it is an appropriate place to investigate how convergence at a continental plate boundary is accommodated both in the presumed brittle upper lithosphere and in the more ductile lower lithosphere and underlying upper asthenosphere. Previous work (e.g. Scherwath *et al.* 2003; van Avendonk *et al.* 2004) has documented in detail the crustal deformation across the continental plate boundary. However, how convergence is accommodated in the uppermost mantle has been controversial. One model, based on the modelling of teleseismic arrivals at a closely spaced line of seismographs across the central South Island, is that upper mantle is converging symmetrically, leading to a symmetric down warp of cold upper mantle into deeper warmer mantle (Fig. 3; Molnar *et al.* 1999; Stern *et al.* 2000). This has been taken to be a presently developing example of the gravity driven Rayleigh–Taylor instability hypothesis of Houseman *et al.* (1981), and Houseman & Molnar (1997). In contrast, a 3-D inversion of teleseismic arrivals (teleseismic tomography) at an array of stations across the South Island, yielded a 3-D *P*-wave image that indicated a ribbon-like high velocity anomaly under the South Island that generally dipped to the west and could be interpreted as demonstrating west dipping subducting mantle under the South Island (Fig. 3. Kohler & Eberhart-Phillips 2002). The latter model was not well constrained due to a lack of teleseismic arrivals and a good azimuthal distribution of events.

The densification and upgrade to broadband of the national seismological array for the South Island and the increase in number of events recorded over an additional 10 yr has encouraged the reanalysis of telesesmic data for the region to derive more accurate 3-D tomographic models of the lithosphere and upper mantle, as well as surface wave models, of the South Island, New Zealand in order to resolve between the two end-member models of continental plate boundary mantle shortening in New Zealand.

2 METHOD AND DATA

Teleseismic tomography is prone to vertical smearing of anomalies and is further plagued by limited sensitivity to the vertical location of shallow velocity anomalies. To overcome these limitations, the teleseismic inversion method used accounts for shallow structure by calculating traveltimes through two initial 3-D models of the crust and uppermost mantle. We then compute tomographic models using two different initial 3-D models. The resulting models have trade-offs between vertical and horizontal resolution. We therefore

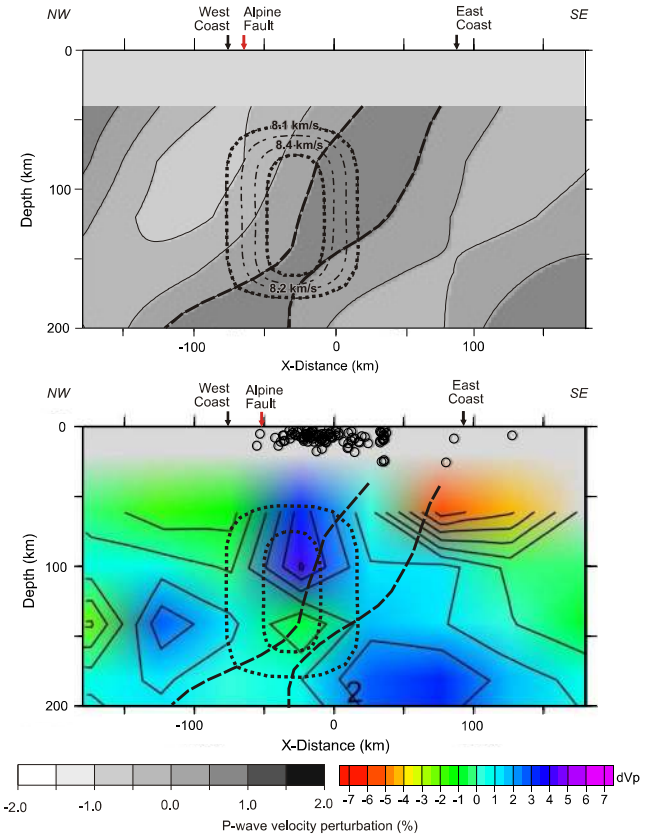

Figure 3. Upper profile shows models of mantle velocity anomalies across central South Island (located by orange line in Fig. 1) used to infer how mantle shortening is accommodated. A localized symmetric upper mantle high velocity body was derived by Stern *et al.* (2000) and shown by the dashed contours (8.1–8.4 km s^{-1} at 0.1 km s^{-1} intervals). A northwest dipping high velocity band was derived by Kohler & Eberhart-Phillips (2002) and is shown by the grey scales contours. Lower profile shows the results from this study (colour image for LET based model) with sample contours of both the Stern *et al.* (2000) model (dots) and the Kohler & Eberhart-Phillips (2002) model (dashes) overlain. Colour bar and grey scale bar shows *P*-wave velocity perturbation (%) for our model and the Kohler & Eberhart-Phillips (2002) model.

compare the results of the different inversions in order to assess consistency (shape and depth extent) in the features of the final velocity models. The first initial model is a local earthquake tomography (LET) model extracted from the New Zealand wide 3-D velocity model ('NZ-wide', Eberhart-Phillips *et al.* 2010) which is based on regional results of Eberhart-Phillips & Bannister (2002) and Eberhart-Phillips *et al.* (2008). The second initial model is a new surface wave model based on the inversion of dispersion data retrieved from noise-correlation empirical Green's functions (EGF). The two crustal models are complementary as the LET model is expected to have better resolution in areas with significant crustal seismicity (e.g. northern South Island and southwestern South Island), whereas the surface wave model is expected to have greater vertical resolution and provide a better constrained crustal velocity model for central and southeastern South Island. We derive 3-D models of *Vp* and *Vs* that define an improved shape and depth resolution for the major features under the South Island region.

The basic data used in the surface wave inversion are continuous waveform recordings from broad-band stations in the GeoNet network (Petersen *et al.* 2011) that were operational between 2008 and 2010. For the teleseismic data set, we supplemented the *P* arrival data set of 56 events used in Kohler & Eberhart-Philips (2002). The seismograph stations used are shown in Fig. 1(lower inset). We selected magnitude >6 earthquakes that provide improved ray path coverage, with epicentral distances greater than 30°, and occurred for a period following the permanent network upgrades (2004–2009). We hand picked *P* and *S* arrival data. In total there were 127 usable teleseismic events (Fig. 1, upper inset) for *P* data, and 61 events for *S* data. For each event, the data were demeaned relative to the average residual at the South Island permanent national seismic network stations.

3 SURFACE WAVE METHOD

We measure fundamental mode Rayleigh wave dispersion from the stacked cross correlation functions of every station pair in the Geonet network. We follow the cross-correlation procedure defined in Stehly *et al.* (2009) to produce the stacked cross-correlation functions for all vertical components. This procedure involves removing instrument responses and then performing cross-correlations of continuous data from mutual time periods. We deviate from the original method by creating day-long correlation functions that are stacked correlations from successive 6-hr correlation windows. These 6-hr correlation windows are spectrally whitened prior to being correlated. We then fold the causal and acausal portions of the correlation to create a positive-time function that resembles the surface wave coda of a traditional earthquake signal. Group velocities are then measured from the folded correlation function with a frequency-time approach which allows for the analysis of the energy contained in the signal at a discrete time for a discrete frequency range. We adapt the filtering and measurement approach from Meier *et al.* (2004) so that it is applicable specifically to shorter-band noise-based dispersion (Fry *et al.* 2010). We measure dispersion between 500 and 25 mHz. The number of data is dependent on frequency, with fewer measurements for the highest and lowest frequencies that we consider.

We invert the group velocity measurements at discrete periods to give 2-D Rayleigh wave velocity maps following the procedure described in Fry *et al.* (2010). The method is based on the inversion scheme used by Deschamp *et al.* (2008) and Darbyshire & Lebedev (2009) to invert earthquake-based dispersion records for isotropic and anisotropic velocity structure. In this study, we use only the isotropic velocity information. We then define a 25 km^2 grid of nodes across the study area. 1-D dispersion curves are created at each of these nodes by sampling each of the period-dependent 2-D maps at that node. These curves are subsequently inverted for shear wave velocity profiles. This is accomplished in a least-squares minimization by fitting a synthetic dispersion curve to the measured 1-D curve at each node. This model is iteratively perturbed until the misfit of the synthetic and input dispersion curves is minimized.

4 TELESEISMIC TOMOGRAPHY METHOD

The teleseismic tomography uses a damped LSQR algorithm similar to that used by Kohler & Eberhart-Phillips (2002). This method uses an initial 3-D velocity model and iteratively perturbs it to reduce the misfit between measured and calculated traveltime residuals. We account for the far-field velocity structure by fitting the traveltime residuals for each event compared to the average traveltime residual recorded on the South Island permanent stations. A grid parametrization with blocks of 50-km horizontal and 40-km vertical

dimension is used. The study area was rotated approximately 40° counter-clockwise to create a simple 50-km Cartesian grid in which the long dimension of the South Island is approximately parallel with the *y*-axis of our grid. Three initial 3-D models were tested, based on a 1-D model (with *Vp* increasing from 8.2 km s^{-1} at 60 km depth to 8.9 km s^{-1} at 360 km depth), the NZ-wide LET (Eberhart-Phillips *et al.* 2010) and the results of the surface wave modelling discussed above. The inversion does not solve for crustal blocks in the upper 40 km. Instead, the 3-D crustal models are used to trace the ray paths from the stations to 60 km depth and to compute crustal traveltimes which are subtracted from the residuals.

The inversions for the 1-D and LET tomographic models uses the NZ-wide model for crustal traveltimes and the 1-D or the LET tomographic models for the deeper part of the starting models respectively. The inversion with the surface-wave initial model uses the surface-wave model for crustal traveltimes and for the subcrustal initial model, although the surface wave model reverts to 1-D below the depth of surface wave resolution at about 100 km depth. A range of damping parameters was tested to determine an appropriate value which provides a reduction in data variance without producing large artefacts in poorly resolved portions of the model. The NZ-wide LET model has uneven resolution related to the earthquake distribution, and it images structure to 300 km depth where there are deep subduction earthquakes in the North Island, but less than 40 km depth in parts of the South Island. Thus we added a secondary damping parameter based on the NZ-wide spread function to damp perturbations in the well-constrained portions. Autolinking between blocks forming the models was also used to increase block-size up to 100 km x × 150 km y (e.g. a group of six 50 km blocks) in sparsely sampled regions. To avoid arbitrary patterns from linking, linking was done in six different ways and the average of those results forms the final model.

As the teleseismic inversion scheme is an iterative approximation and does not solve the inversion problem explicitly, we do not calculate a resolution matrix. However, an estimate of the resolution of the modelling can be derived from the distribution of data as shown by block hit count for *P* and *S* waves (Fig. S1). The island is narrow and the larger proportion of rays are from earthquakes to the northwest and therefore sample the northwest part of the South Island. Thus the eastern South Island has poorer resolution than the western side. However, the deeper structure in the east is better imaged than in earlier models because of the additional data and by using 3-D initial crustal models in the inversion. Below 260 km depth, resolution is low directly under the South Island as the ray paths are coming up from either side, but resolution under the margins of South Island is better (Fig. S1). There will be smearing along ray paths in the offshore areas because of the narrowness of the island (∼200 km). Thus, while there is adequate data coverage to discern deep features offshore, they may be smeared upward. Similarly other features may be smeared downward toward the northwest or southeast side along the ray paths.

In order to evaluate the reliability of the inversion results, we make a rigorous synthetic test model (Figs S2–S4) which has many of the key tectonic elements that we infer for the region. It was created on a finer grid than the 50-km-block teleseismic grid such that the inversion could never derive fully the true model. Tectonic elements such as subducting or remnant slabs have sharp velocity gradients and shapes that can be defined on a finer grid than the 50 km inversion grid. Hence we aim to explore how actual features' shapes and velocity gradients might be imaged. The test model had velocity anomalies of four percent, and is shown in Fig. S2. The major features of the test model are derived by the inversion with velocity anomalies centred at correct locations. However, there is smearing along ray paths and velocity gradients are broadened. Because the teleseismic tomography uses relative residuals, the actual velocity perturbations derived by the inversion may be less reliable than the location of the gradients.

5 RESULTS

5.1 Surface wave inversion model

The surface wave velocity inversions provide a 3-D *Vs* model. The model is shown for several depth slices on a 25 km grid in Fig. 4 and as depth profiles in Fig. 5. The teleseismic *P* data set is much larger than that for *S* waves, and thus this surface wave model has been converted to *Vp* assuming a *Vp*/*Vs* ratio of 1.75 for the crustal structure model used in the *Vp* inversions. This is an average *Vp*/*Vs* based on previous LET results, and while undoubtedly imprecise in some areas, the *Vp*/*Vs* conversion enables incorporation of the surface wave results into the teleseismic tomography. Below about 55km, the surface wave results are not well constrained, however, they are still useful in making a smooth transition between the surface wave sensitivity and teleseismic sensitivity in the combined modelling.

Several general features of the *S*- and *P*-wave velocity fields show clearly through a significant depth range. Low velocities occur under northwest South Island (Nelson region $x = -50$, $y = 250$, region Ac—Figs 4d and 5a), extend down from $Z = 21$ to 45 km (i.e. through the mid-lower crust) but become a positive velocity anomaly, Am, at 55–75 km depth. Region Bc (Figs 4c, 5b and c) delineates shallow low-velocity rocks in the Canterbury region ($x = 100$, $y = 50$, $Z = 0$–21 km) that do not extend into the lower crust ($Z = 27$ km). The low, near surface velocities may be associated with the thick sediments forming the Canterbury Plains (up to 1.5 km, Forsyth *et al.* 2008). A relative low velocity (7.4 km s^{-1}) is derived again at upper-mantle depths ($Z = 55$–75 km), in central east South Island, (from $x = -25$ to >100, $y = 100$ to -50, region Bm in Figs 4g, 5b and c). It is possibly 20 km thick, but the lower edge is not well constrained. There is a smaller low-velocity upper-mantle region near Dunedin ($x = 150$, $y = -225$) at 75 km depth (C in Figs 4h and 5e).

A low velocity region ($Vp \leq 6.5$ km s^{-1}) extends across central South Island (D, Figs 4c–e, 5d and e) from the mid-west coast of South Island (Mount Cook region $x = -50$, $y = -100$) to the South Otago coastline in the east ($x = 100$, $y = -300$). It is more pronounced at shallow depths ($Z = 21$, region D in Fig. 4c), and continues to the south in a more subdued form to the base of crust and the uppermost mantle ($Z = 35$ km, region D in Fig. 4e). Beneath this, high velocity mantle rocks ($z = 55$ km, $Vp > 8.25$ km s^{-1}) occur in a NW–SE band across central South Island (E, Figs 4g, 5c–d) from Mt Cook ($x = -50$, $y = -50$) to North Otago (Dunedin, $x = 100$, $y = -200$), but are not imaged at 75 km depth

A high velocity mantle region, (region F in Figs 4h and 5e), under southwestern South Island was also derived in LET studies (Eberhart-Phillips *et al.* 2010) although it was only well constrained on its western side by the deep Fiordland earthquakes. The surface wave data now define a sharp eastern boundary ($x = 80$) to this feature at depths > 55 km under southeast South Island ($y = -300$).

Over most of the South Island, relatively normal lower crustal and uppermost mantle velocities of ∼7.0–8.0 km s^{-1} are derived at depths of 25–40 km (Figs 4d–f).

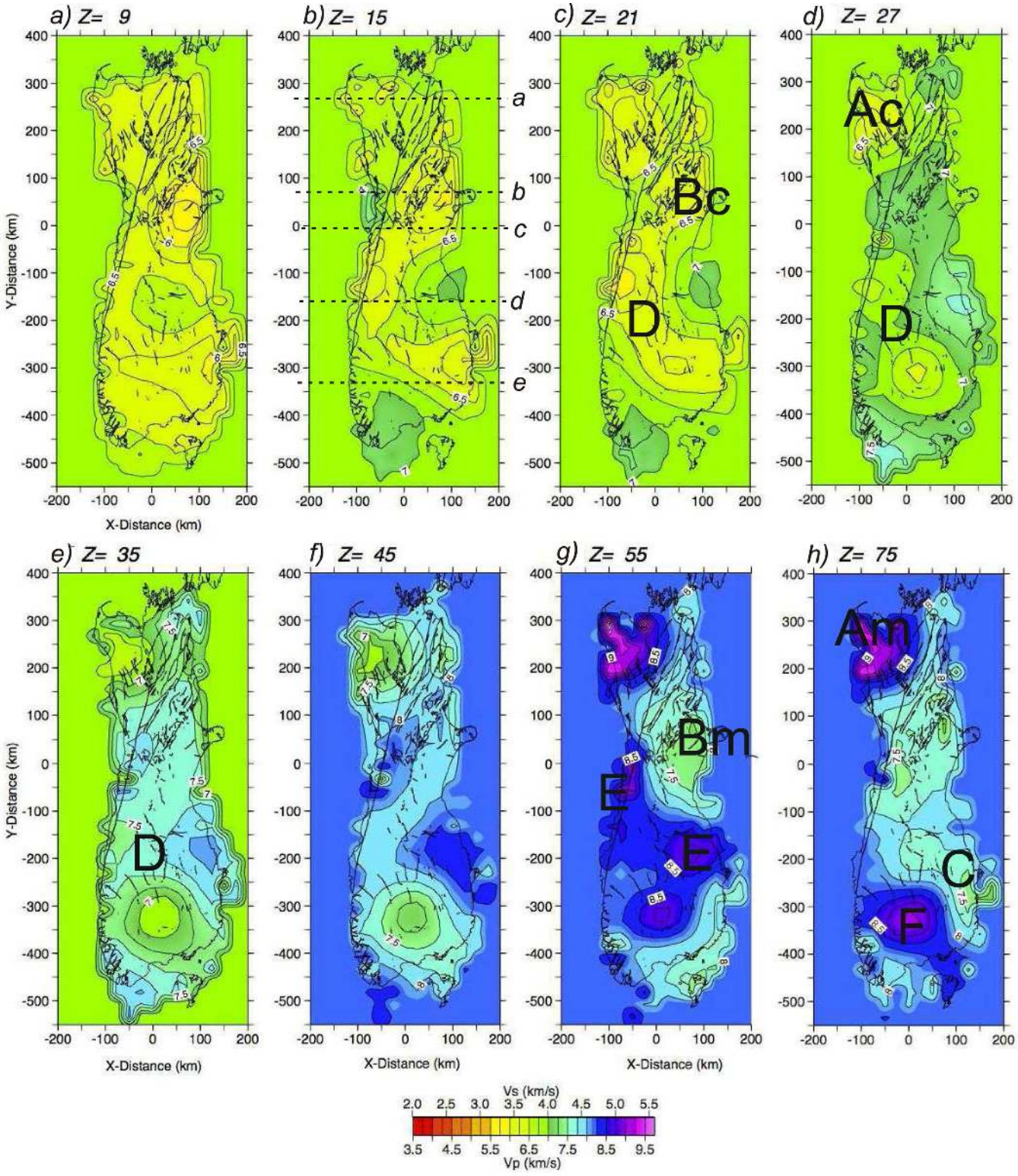

Figure 4. Depth slices through the surface wave derived crustal model in this study. Black letters (A–F) are used to locate regions discussed in the text. Depth (Z in km) of the slice is annotated at the top of each slice. Black dashed lines labelled *a* to *e* on slice 'b' ($Z = 15$ km) are the locations of the profiles in Fig. 5. Fig. 5. Cross-sections through the surface wave crustal velocity model. The model extends to 80 km depth but resolution diminishes significantly below about 60 km. Black letters (A–F) are used to locate regions discussed in the text. Short red lines are mantle receiver functions interpretations that lie within 25 km of the profile (after Spasojevic & Clayton 2008). The coastline of South Island is marked by short vertical lines annotated by 'c'.

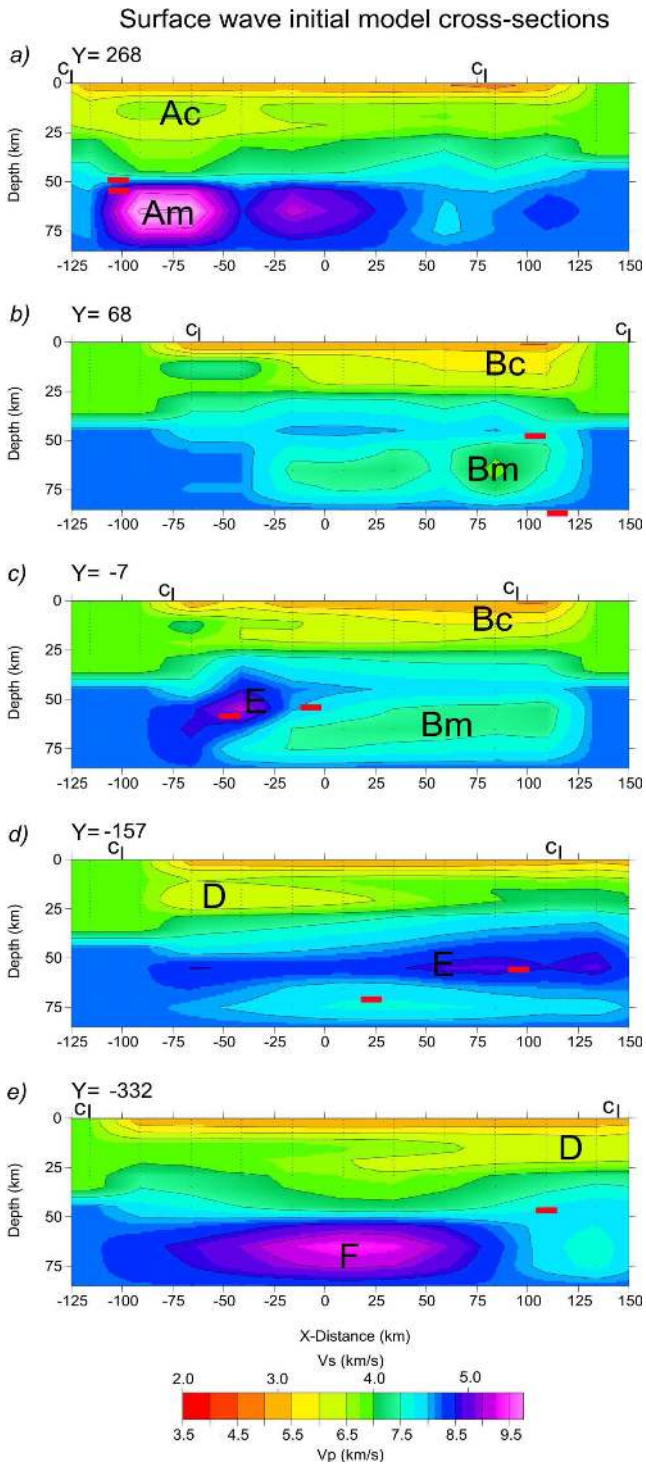

Figure 5. Cross-sections through the surface wave crustal velocity model. Sensitivity diminishes significantly below 60 km. Short red lines are mantle receiver function interpretations that lie within 25 km of the profile (after Spasojevic & Clayton 2008). The coastline of South Island is marked by short vertical lines annotated with 'c'. Bold annotations (A–F) refer to features that are discussed in Section 5.

5.2 Teleseismic inversion models

We show the *P*- and *S*-wave velocity models on six horizontal slices, crossing the models at increasing depths from 60 to 260 km (40-km-depth spacing). The 3-D *Vp* and *Vs* models derived include three *P*-wave 3-D models (Figs 6, 7 and S5) and two *S*-wave models (surface wave based and 1-D model based, Fig. 8). There is little resolution below 260 km depth although models were computed to 340 km depth. An indication of the resolution of the inversion can be assessed from plots of the ray hit-points (Fig. S1). Both *Vp* and *Vs* show a number of consistent features for the lower lithosphere and uppermost mantle of the South Island on all 3-D models (Figs 6–10 and S5). Only the surface wave and LET based 3-D tomographic models will be discussed in detail, other plots are in the Supporting Information files for completeness. The data used in the teleseismic analysis are from a variety of azimuths. As such, although the crustal rocks and the lithospheric mantle are known to be anisotropic, the inversion of data from a wide range of azimuths will give a near isotropic velocity model.

A high velocity body 'A' is imaged at 60 km depth under northwest Nelson ('N' in Fig. 1, $x = -75, y = 250$—coordinates given in Figs 6–9), similar to that found on the crustal model derived from surface wave inversion. A high velocity body 'B' is imaged from about 60 km depth under the northern two thirds of central South Island (along $x = 0$ to –50 in Fig. 6a). At greater depths (100 km) this high velocity body 'B' becomes stronger and extends to north and south (along $x = 0$ to -50 in Figs 6b, 7b and 10c) and extends south of the South Island ($y = -400$, $x = -50$, Figs 7b, c and 10c). On the surface wave based model, this high velocity core stops at $y = -100$. The velocity anomaly is largest in the north ($y > 250$ km) and is weaker at about $y = -100$ and -300 km.

In the north ($y > 200$), shallow ($z < 100$ km) seismicity coincides with the centre of the high velocity region (Figs 7b, 9a–d) marking the subducting Pacific Plate. Below about 150 km, this velocity high apparently splits south of $y = 350$ (north end of South Island) with the main high velocity zone ('C' in Figs 6d and 7d) along $x = -125$ and a minor high velocity zone along $x = 0$. Below 120-km depth the seismicity dips steeply and follows the central inclined high velocity zone that corresponds to the subducting Pacific mantle while the western more shallowly dipping high velocity region (C, Fig. 9c) may have another cause.

North of $y = 0$, the western dipping high velocity body (C, dip $= 40^\circ$ approx.) lies west of the steeply dipping slab seismicity profiles at $x = -150, z = 180$ to $x = -200, z = 260$ (Figs 9a–d). In contrast to the subducting Pacific Plate, the western feature is most pronounced below 150 km depth, and is separate from the Pacific slab in the LET results (Figs 9b and d). Thus it may be a feature below 150 km depth with smearing upward. Such a feature was tested in the synthetic model with high-velocity below 260 km depth (Fig. S2f), and it was imaged with some vertical smearing (Fig. S4a). The western shallow dipping high velocity body (C) continues south of where the seismicity ceases and appears to extend deeper and is discernible, but poorly constrained, to below 340 km depth. This western high velocity zone continues to the north below 200 km and terminates in the north ($y > 500$ km), forming an extensive, dipping, high velocity mantle region west of southern North Island and northern South Island ($50 < y < 500$ km, $x = ->100$ to -300 km: Figs 6d, e, 7d and e).

South of $y = 0$, another west dipping high-velocity body (D, Figs 6f, 7e, f, 9i and j) occurs from $x = -200, z = 200$ to $x = -300, z = -300$. This is most prominent at $z = 220$ and the deeper image may be partially the result of smearing. Although it appears detached from the west dipping feature north of $y = 0$, they may be the same feature with a break or bend in the body in the south. Further south, $y = -175$ to -500, a subdued higher velocity body occurs under southwestern South Island and dips steeply to the west

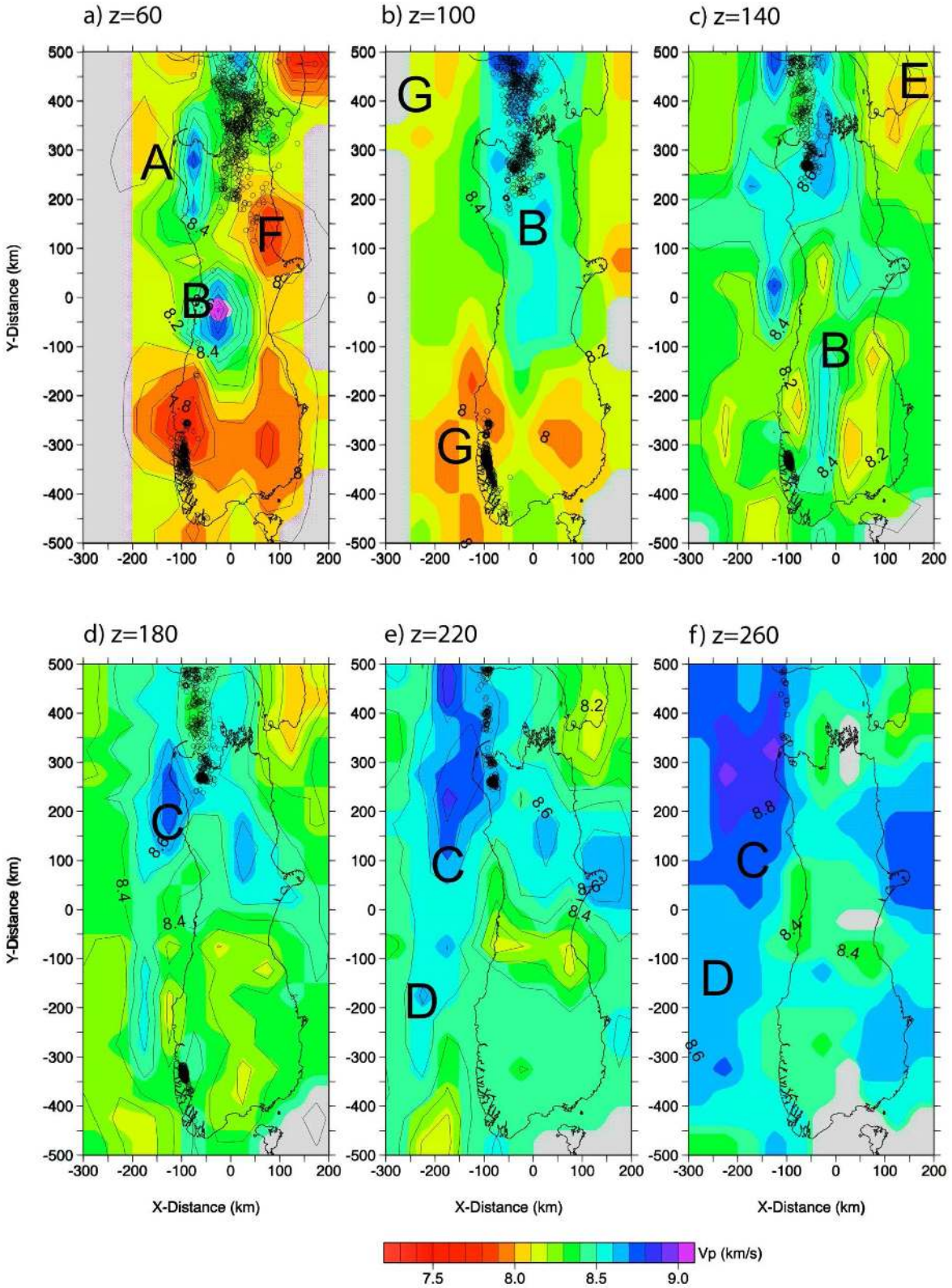

Figure 6. Depth slices from the final 3-D *Vp* model based on the surface wave initial model shown at depth intervals of 40 km between 60 and 260 km depth. Solutions are obtained by averaging six inversions with different block linkages. Plots are masked where less than 20 rays traversed the blocks. Black letters (A–G) are used to locate regions discussed in the text. Deep epicentres for earthquakes between 2001and 2010 and with $M > 3$ are shown by black circles.

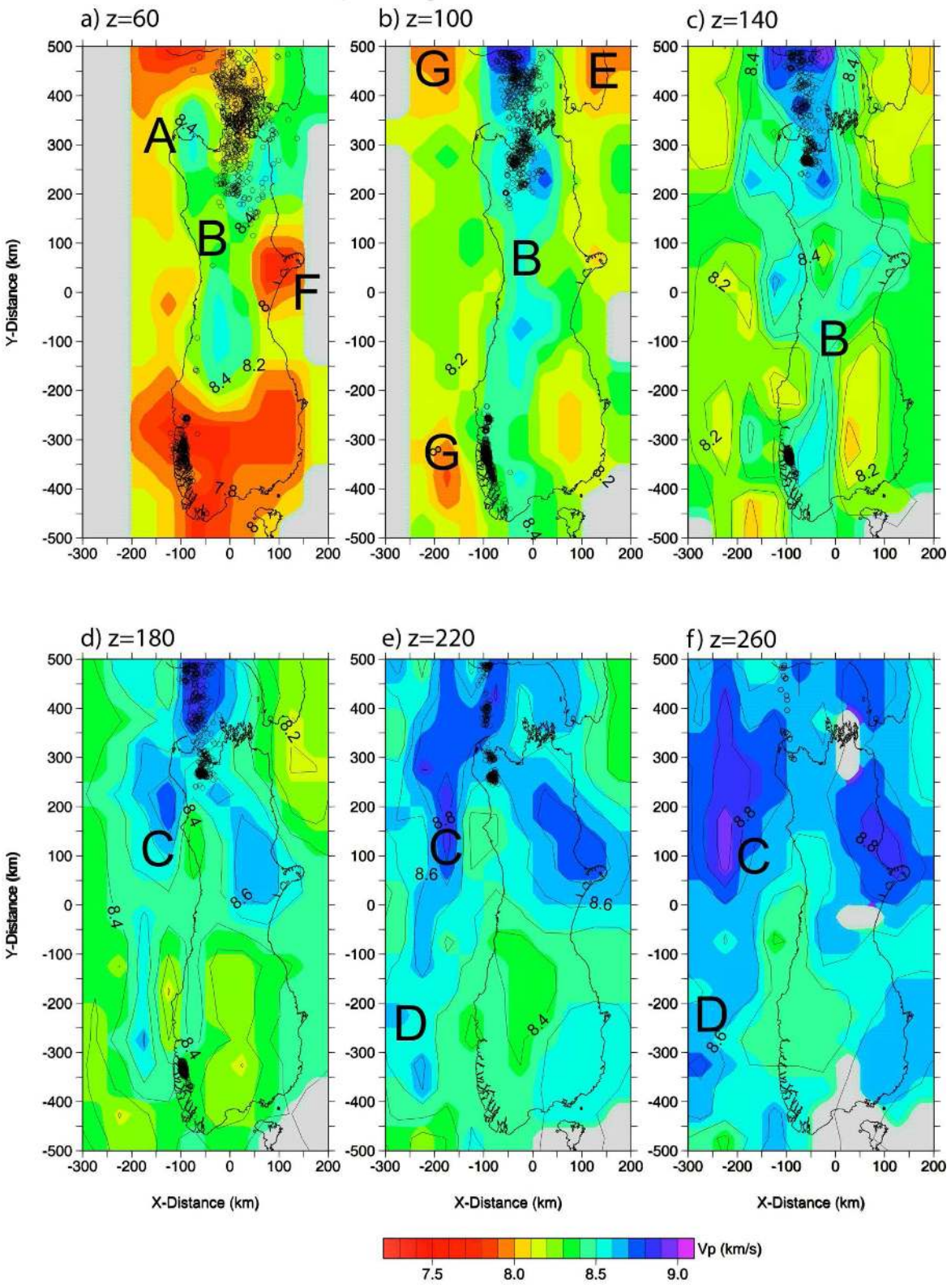

Figure 7. As for Fig. 6 but with LET initial model and crustal correction.

from $x = -50$ to -150, $z = 150$–220 (Figs 9g–j). It is present in all three models.

Several low velocity regions are conspicuous. A low velocity upper mantle anomaly occurs under the subducting Pacific Plate of eastern North Island from 60 to 180 km depth (region E, Figs 6c and 7b). Further south, at 60 km depth, a strong low velocity region (region F, Fig. 6a) coincides with the Canterbury region. The latter occurs on the deeper depth slices of the surface wave inversions

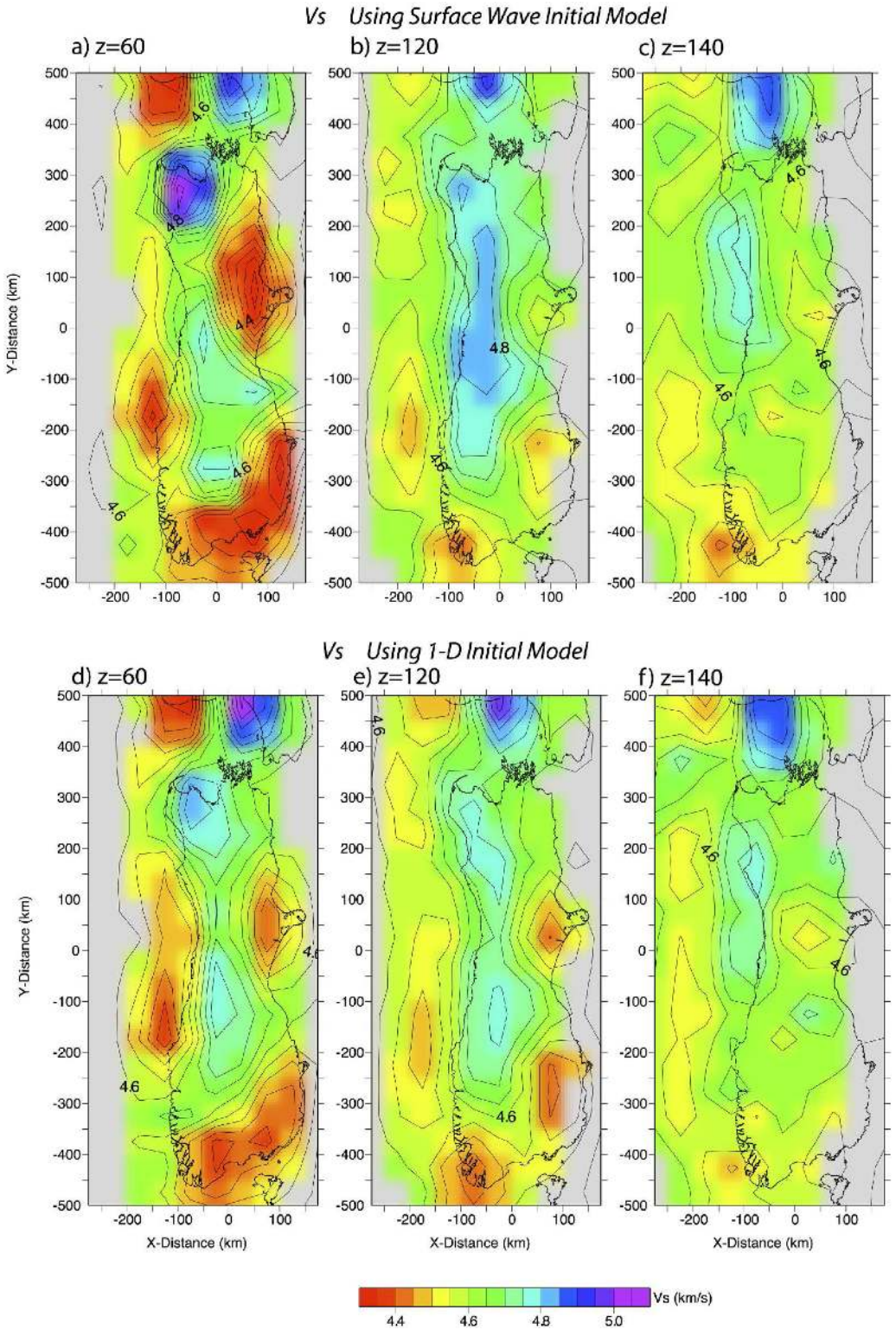

Figure 8. Depth slices through the *Vs* velocity models resulting from using the initial surface wave model (a–c) and a 1-D starting model (d–f).

(Fig. 4) and demonstrate that it lies in the upper mantle and is not an artefact generated by incomplete compensation for the thick shallow upper crustal sediments (Forsyth *et al.* 2008) that occur there. The west of North Island, the south of the South Island, and west of Stewart Island (region G, Figs 6b and 7b) are also marked by relatively low upper ($z = 60$ km) mantle velocities ($Vp = 8.0$ km s^{-1} approx.).

6 DISCUSSION

6.1 Crustal and lithospheric mantle models

The new surface wave lithospheric model provides additional insight into the broad structure of the lower crustal and upper mantle underlying South Island, although its horizontal resolution is

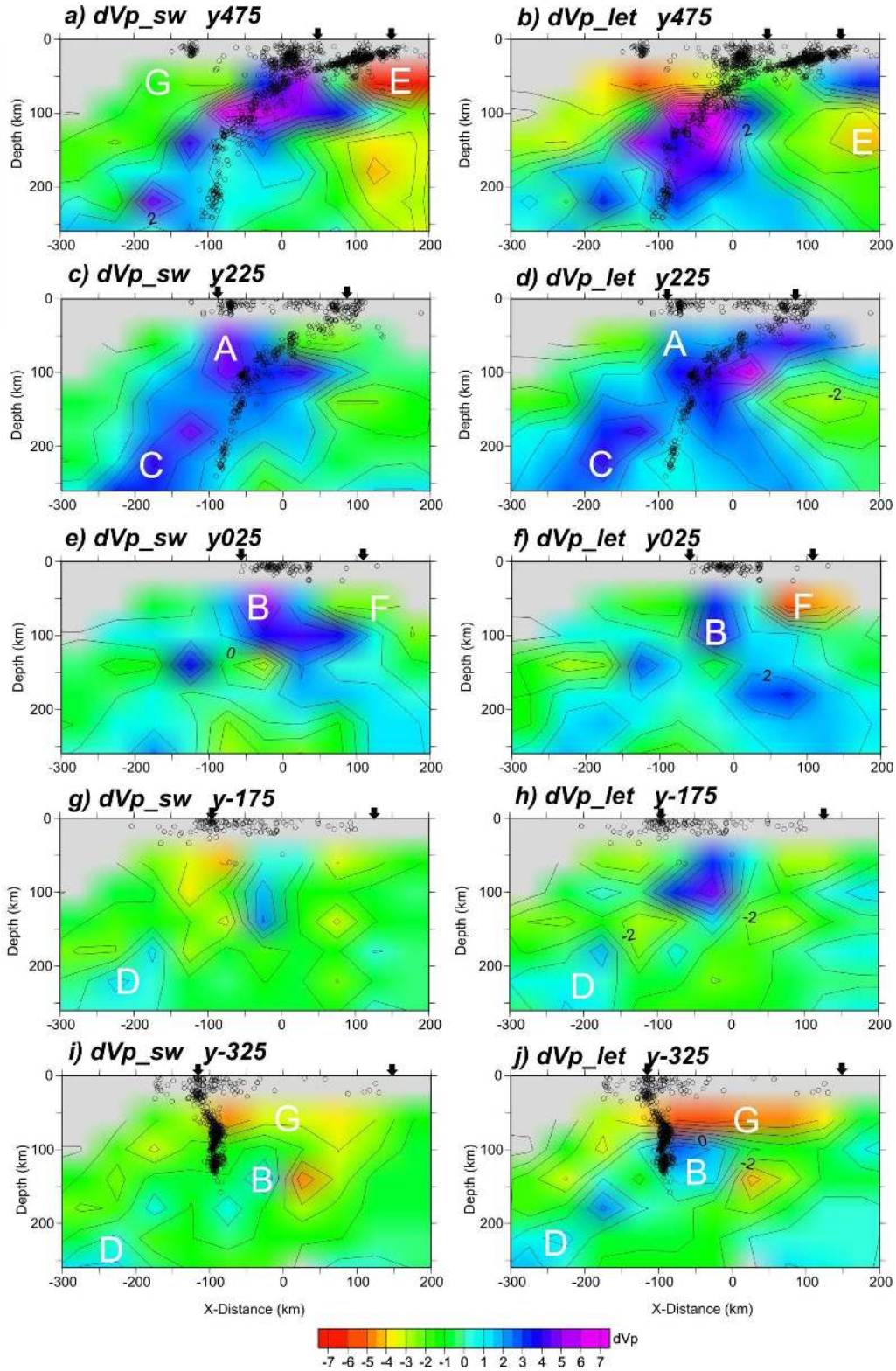

Figure 9. Cross-sections of d*Vp* (relative to a 1-D South Island model) based on *Vp* tomography using a surface wave initial model (left-hand panels) and a LET initial model (right-hand panels). Hypocentres as in Fig. 8 are shown by black circles. The coastline of South Island is marked by short vertical arrows. White letters (A–G) are used to locate regions discussed in the text.

limited with increasing depth as the modelled periods range up to 40 s (∼130 km wavelength). The low crustal velocities (Ac, Fig. 4d) in the NW Nelson region are spatially related to the extensive granites that occur there (the Palaeozoic Karamea and Mesozoic Median Batholiths) and are intruded into the Palaeozoic Takaka and Buller Terranes of the Western Province rocks (Australian Plate; Fig. 2). The spatially coincident local high velocity mantle ($Vp > 8.5$ km s^{-1}, Am in Fig. 4h) immediately underlying Karamea Batholith (Fig. 2)

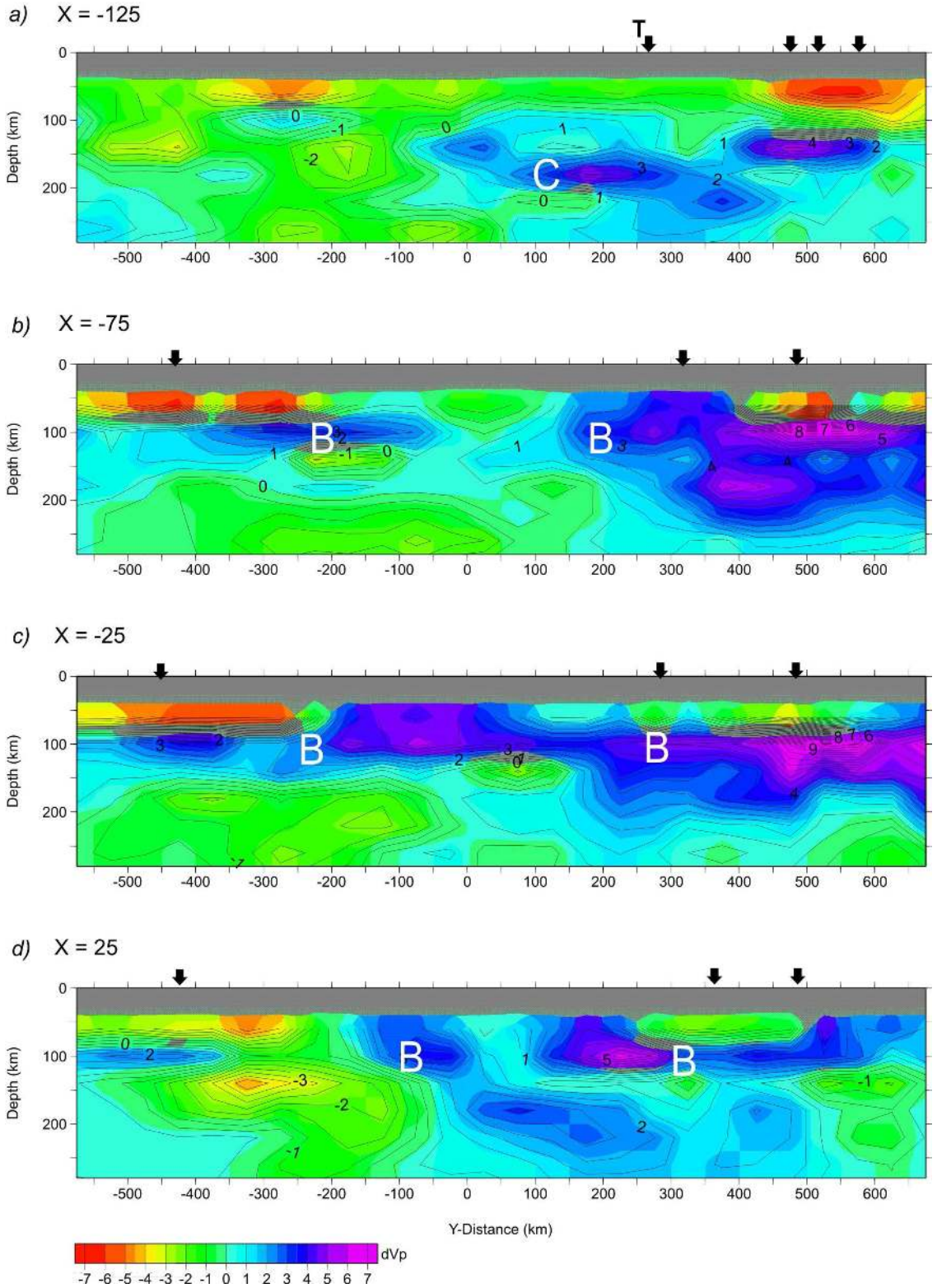

Figure 10. Cross-sections (at $X = -125, -75, -25$ and 25 km) as in Fig. 9 showing dVp along the South Island based on the LET initial model. The coastline of South Island is marked by short vertical arrows. 'T' on the uppermost profile marks where the profile just touches the South Island coast. White letters B and C are used to locate regions discussed in the text.

is intriguing. Eberhart-Phillips & Bannister (2010) propose that it may document the mafic residual from the fractionated crust–mantle that gave rise to the extensive granites, and reflect the mantle depletion of light elements. However, the Median Batholith in the southern part of South Island is underlain by the low velocity mantle region suggesting that an upper-mantle residue may have been more mafic for the older, Palaeozoic, Karamea granitoids in the north.

A crustal low velocity region is associated with the thick sediments that occur in the Canterbury region, (Bc, Fig. 4c). This region is underlain by a low velocity upper-mantle layer at about 50–100 km depth (Bm in Figs 4g and 5b, c), the top and base of which are similar in depth to some of the upper mantle *P* to *S* conversions derived from receiver function analysis by Spasojevic & Claydon (2008) in this region. The stations used for the receiver function analysis are shown in Fig. 1, with the depth to the *P* to *S* conversions shown in Fig. 5. There is not a consistent association as the conversions occur sometimes near the base of the low mantle velocity body and sometimes near the top, and are spatially more extensive.

In the Fiordland region, several studies (Smith & Davey 1984; Eberhart-Phillips & Reyners 2001; Eberhart-Phillips & Bannister 2002) have detected a high velocity body to the east of the Fiordland subduction zone. The surface wave based velocity model defines an eastern boundary to this high velocity zone (region F in Fig. 4h), which appears to be distinctly separate from the high velocity uppermantle zone (region E in Fig. 4g) that crosses southern South Island from Mount Cook to Dunedin and is spatially associated with the Alpine Schist.

The Hikurangi Plateau, a large igneous province, impacted into the Cretaceous subduction zone along the Pacific margin of Gondwana and partially subducted under the continental margin (Chatham Rise). Since the onset of Tertiary subduction under New Zealand (Hikurangi margin), the Hikurangi Plateau has also been subducting under eastern North Island and northeastern South Island. Based on seismicity and a high *Vp* ($\geq$8.5 km s^{-1}) for the deeper part of the plateau, Reyners *et al.* (2011) have proposed that the subducted Hikurangi Plateau extends under most of the South Island. The existing *Vp* data is very limited under central South Island due to limited active source crustal seismic experiments and low rates of seismicity for local seismic tomography. The new surface wave crustal model (Figs 4 and 5) shows *Vp* velocities of 8.5 km s^{-1} or greater at depths of 60 km or less under parts of South Island west and south of Canterbury ($y = 0$, region E in Fig. 4g) that could correspond to the subducted Hikurangi Plateau interpretation of Reyners *et al.* (2011). This high velocity region extends along the plate boundary and from the central west coast of South Island near Mount Cook to the Dunedin region and northern Fiordland (Fig. 4). Further south, smaller lower crustal velocities occur under the Caples to Brook Street terranes of the Eastern province (region D in Figs 4c–e) suggesting that the Hikurangi Plateau did not extend this far south. The teleseismic models show *Vp* less than 8.5 km s^{-1} down to 100 km depth, suggesting that the Hikurangi Plateau does not extend any further south than the western extension of the Chatham Rise. However, the conflicting interpretation may arise from the vertical smoothing of velocities when derived for a 50 km grid

7 UPPER-MANTLE VELOCITY MODELS

The teleseismic tomographic models show three major features: (i) a horizontal core of high velocity mantle rocks extending at a depth of about 100 km from the subducted Pacific Plate in the north to the central south coast of South Island, with a trend at about 10–15° east of the surface trace of the plate boundary (region B in Figs 6, 7 and 10); (ii) a 100-km-wide zone of high velocity, presumably cold, mantle dipping approximately at about 40° to the northwest to depths in excess of 250 km, and extending at about 50 km depth from Marlborough in northeast South Island to central South Island and at greater depth to west of South Island (regions C and D in Figs 6 and 7). It supports, in general, the major findings of Kohler & Eberhart-Phillips (2002) and (iii) low mantle velocities west of North Island and across the southern half of South Island (region G in Figs 6b and 7b).

The 3-D *Vp* and *Vs* tomographic models delineate a high velocity core along the longitudinal axis of the South Island, extending from the high mantle velocities associated with the present subduction in the northeast to the central south coast of South Island (B, Fig. 10c). This core is quite restricted in width, and, although the model grid is fairly coarse to define it in detail, the velocity gradients derived indicate a core about 50 km in depth extent and 100 km wide, that lies at about 75–125 km in depth. The velocity anomaly is strongly focused at 100 km depth and is more strongly defined in the south in the LET based model. The *Vs* anomaly extends further south as a strong feature than does the *Vp* anomaly (Figs 6 and 8). There is no strong, cross strike dip associated with this body although there is a subdued west dipping component that may indicate some mantle subduction. The azimuth/strike of the core is oriented at about 10–15° anticlockwise from the present surface plate boundary (Alpine Fault), similar to the Bouguer gravity azimuth (Beaumont *et al.* 1996; Gerbault *et al.* 2002; Scherwath *et al.* 2006; Fig. 1). Scherwath *et al.* (2006) derive a 3-D gravity model for the upper mantle. Their model is only well controlled in central South Island where it shows major widening and deepening to the southwest (75–150 km depth), suggesting mantle extrusion to the south. They derive an asymmetric model that is thicker to the northwest and thus consistent with a northwest dipping high velocity (density) body. Seismic refraction measurements (Bourguiguon *et al.* 2007) and numerical modelling (Gerbault *et al.* 2002) show crustal thicknesses increasing to the southwest, which Gerbault *et al.* (2002) model as largely due to thickening of the lower crust by southward extrusion of the ductile lower crust that ceases at the southern limit of the plate boundary offset (central Otago) and is caused by transcurrent plate boundary motion. The 3-D velocity models show that a high velocity mantle anomaly (the core) underlies this crustal thickening. However, the mantle core also continues further south indicating that it is not related solely to crustal thickening and is probably primarily a response to plate convergence that is symmetric in character.

The high velocity core appears to run to the southwest from about 45°S at 50 km depth to the southern margin of South Island at 120 km depth and further south where it aligns with the southeastern end of the Puysegur trench and the transcurrent faulting of the Macquarie Ridge (Fig. 1). This alignment of the high velocity mantle zone along the longitudinal axis of South Island suggests that it may be caused by convergence along the former plate boundary that occurred along this axis. Kamp (1986) documented an extensional rift, the Challenger rift, that extended from the Emerald Basin spreading centre south of South Island, through an active fault zone that ran along the present eastern margin of the Fiordland block and the central South Island and northwest Nelson to off shore Taranaki. It was active from about 40 to 25 Ma when extension reversed and strike slip motion with minor convergence occurred, leading to an eversion of the rift basins along this boundary. A steady movement in the pole of rotation for the Pacific–Antarctic Plate boundary led to a subsequent increase in convergence and the development of the Hikurangi subduction zone in the north and the Puysegur subduction zone in the south. The convergence across the older plate boundary would have developed a mantle anomaly, a dense body of cold lithospheric mantle emplaced in the asthenosphere, that is suggested to be the cause of the high velocity uppermost mantle body that is imaged in the seismic data. This body follows the older

plate boundary from the old Emerald Basin spreading ridge—the transcurrent Macquarie Ridge—to the south end of the Hikurangi subducting plate. We suggest that present mantle convergence is focused on this older, probably weaker, mantle plate boundary, and that this boundary has provided a focus for the channelling of the extruded lower crustal material to the south to give the regional gravity low. The greater extent to the south of the strong anomaly in *Vs* compared to *Vp* suggests that the core rocks to the south may possibly be more dehydrated consistent with the lesser influence of younger convergent tectonics in the south.

A major aim of the present study was to differentiate between the two models of how mantle convergence is accommodated during continental collision, as is happening in central South Island. Our results of a high velocity upper-mantle core under central South Island ($y = 25$ to -100) that is shallow and localized (75–125 km depth), show no clear continuous dipping slab below 125 km depth. Furthermore our seismic models do not show a symmetric high velocity mantle depression to depths of 150 km and greater under central South Island (Fig. 3a), as has been proposed by Stern *et al.* (2000) from the modelling of teleseismic delays. Instead, a similar localized but shallower and broader body is imaged in the surface wave based teleseismic model, and both our teleseismic inversions show a subdued dipping or deeper high velocity body to the northwest of this shallow feature (Fig. 3b). The single event forward modelling technique of Stern *et al.* (2000) could not discern such secondary high-velocity features which also influence the residuals. Our seismic models could be interpreted as indicating some process of successive underplating of subducting mantle, but the images are not detailed enough to speculate further. The teleseismic delays measured by Stern *et al.* (2000) show an advance across the South Island that has two parts: a smaller western part of about 0.8 s, that is modelled remarkably closely by the crustal structure variations (their Fig. 5), and a central part of about 0.7–1.0 s. Inspection of the ray tracing in their figs 9 and 12(d) suggests that the central part of the anomaly may be fitted by a west dipping body. If true, this has important implications as it would indicate no or very localized low velocity crust in the vicinity of the Alpine Fault for seismic energy propagation up from the west at an angle of about 70° to the horizontal. A low crustal velocity in the Alpine Fault region is well constrained by active source measurements for horizontally travelling rays. This interpretation indicates that crustal anisotropy in this region has a fast direction along at approximately 70°NW dip direction and slow direction horizontal. This would be compatible with anisotropy based on near vertical fractures. Although all models are poorly constrained in detail, the body derived by our inversion lies between these two end-member models.

7.1 A Cretaceous palaeo subduction zone

The western high-velocity NW dipping zone underlying western South Island is more shallowly dipping than the present subducted plate, lies west of the Pacific Plate subduction zone in southern North Island and northern South Island, and is most prominent below 150 km depth in the vicinity of a sharp change in dip of the downdip seismicity trend (region C and D in Figs 6, 7 and 9a–d). The teleseismic tomographic models show a 100-km-wide zone of high velocity mantle, dipping approximately at about 40° to the northwest to depths in excess of 250 km, and extending along strike at about 50 km depth from Marlborough to central South Island. South of central South Island, this west dipping high velocity zone is deeper and offset westward. The seismicity in northern South Island lies towards the top of a high velocity zone, as is normal with subduction zones, and against which the western dipping zone abuts. As the seismicity dies away towards the south, so does the deeper part of this subduction associated high velocity anomaly. In contrast to the North Island subducted plate, no high velocity anomaly is derived for the subducting Tasman Sea lithosphere under Fiordland in the southwest of the South Island (Figs 9i and j), a similar result to that found by Eberhart-Phillips & Reyners (2001). A low mantle velocity is derived for this region and inferred to result from the young age of the subduction.

The western high-velocity dipping zone is inferred to be imaging a remnant cold mantle slab marking an older subduction zone. Two main events are possible. The first is subduction under South Island of the western part of the early Tertiary extension that formed the Emerald Basin south of South Island (Sutherland *et al.* 2000). This would however have been directed eastwards under the proto Alpine Fault Plate boundary and therefore have the wrong dip direction. The second event is subduction under the Gondwana margin prior to its cessation about 100 Ma. This subduction event ceased with the arrival of the Hikurangi Plateau at the Gondwana margin about 105 Ma (Davy *et al.* 2008) and the break-up of New Zealand and Australia from Antarctica commenced. In this case, the high velocity zone could be an approximately 600-km-long remnant of the former subducted Cretaceous Plate that detached when subduction ceased. Melhuish *et al.* (2005) observe upper-mantle reflectivity at depths of 50–140 km in active source seismic data off central west coast of South Island that may be related.

The present plate boundary through New Zealand lies along the western margin of the Hikurangi Plateau and this may explain the change in depth to the top of the west dipping velocity anomaly. Our preferred interpretation of the western dipping body is that it is remnant subducted slab under the Gondwana margin that has undergone some clockwise rotation resulting from the 800 km offset of the New Zealand lithosphere during the past 40 Ma (Sutherland 1999) and that the gap to the top of the feature in the south is a result of the influence of the Hikurangi Plateau during the stalling of subduction at the Gondwana margin. The juxtaposition of the present subduction against this old, presumably cold, former subducted lithosphere during Tertiary transcurrent plate movements may be the cause of the increased dip of the present subduction zone to near vertical under Marlborough (NW South Island) at a depth of 120 km. An alternative explanation is that the increased dip may mark the downdip end of the buoyant Hikurangi Plateau as proposed by Reyners *et al.* (2011). The subducted slab will also be influenced by the presence of the adjacent old remnant slab, as it would greatly perturb the asthenospheric flow patterns and limit flux of slab dehydration fluids. This west dipping high velocity mantle zone appears to be offset to the west under the central South Island, which may be related to the southern limit of the underthrust Hikurangi Plateau.

7.2 Gondwana upper mantle

The upper-mantle low velocity region (G, Figs 6 and 7) with *Vp* (7.8–8.1 km s^{-1}) and *Vs* (4.4–4.6 km s^{-1}), extends to mantle depths of about 120 km for a large part of the northwestern and southern continental parts of the region. The Canterbury region is also marked by low *P*- and *S*-wave velocities that extend to depths of about 100 km. These are unlikely to be artefacts as the surface wave starting model defines the surface sedimentary cover well. In addition, similar relatively low upper-mantle velocity regions occur

under the central west coast of South Island, where thick Tertiary–Quaternary sediments up to 4 km thick also occur (Nathan *et al.* 1986; Davey 2010), and across to the southeast coast. The region coincides with the crustal Caples, Muruhiku, Takaka, Buller terranes of pre-Cretaceous age (Fig. 2). The region is presently bounded by Tertiary oceanic lithosphere in the southwest and northeast that formed during the break-up of New Zealand from Australia and Antarctica during the Late Cretaceous and Early Tertiary (Fig. 1) and is transected by Tertiary Plate boundary processes. Reconstructions of the NZ region back to the pre-break up of Gondwana about 80 Ma (Sutherland 1999) shows that these areas were adjacent and formed the inner margin of Gondwana and we therefore interpret them as documenting the continental lithosphere of the Gondwana margin.

An alternative interpretation for the low upper-mantle velocities under the Canterbury region (region Bm, Fig. 4g) is that they are related to the Miocene and younger volcanism that has occurred on Banks Peninsula. The Dunedin region, with volcanism of similar age, has low *Vp* in the surface wave model (Fig. 4h) and low *Vs* in the surface wave based teleseismic *Vs* model (Fig. 8), and has a broad regional velocity reduction in the *Vp* models. The synthetic model results (Fig. S5d) also only derive a subdued velocity low under Dunedin. Although seismic and helium isotope data (Godfrey *et al.* 2001) suggests thermal anomalies at lower crustal-upper mantle depths, these are only in the local Dunedin region. All of the teleseismic *Vs* and *Vp* models and the surface wave model (Fig. 4g) show a band of moderately high velocity separating the low velocity mantle underlying Canterbury and south of Dunedin.

8 CONCLUSIONS

The inversion of surface wave data for the South Island of New Zealand provides improved *Vp* and *Vs* models for the crust and uppermost mantle. The major contributions are in constraining the eastern boundary of the high velocity uppermost mantle east of Fiordland, that forms part of a high velocity, presumably cold, mantle core to the South Island, a low velocity upper-mantle body under eastern central South Island that has been imaged in part by receiver function studies, and the confirmation of low velocities in the crust associated with the Karamea and Median Batholiths of northwest Nelson and their underlying high velocity (inferred depleted) mantle.

Starting from crustal velocity models based on local earthquake tomography and surface wave inversions, the inversion of teleseismic data into South Island has defined the broad mantle velocity distribution under the South Island and its margins to depths of about 260 km. The resulting velocity images have been interpreted to show a linear high velocity core through South Island at depths of about 100 km from the subducting Pacific Plate in the north to the central south coast of the South Island and possibly on to the transcurrent plate boundary forming the Macquarie Ridge. The velocity anomaly is interpreted as caused by lithospheric mantle convergence that is depth constrained and follows the thickened crust underlying the South Island and the older (25 Ma) plate boundary through the region. Even if the resolution of our models in this region is not high enough to unequivocally define whether the convergence is symmetric or underthrusting, gravity-driven drip like features that are 3-D in character or extend to 150 km or more in depth are unlikely. West dipping zones of high velocity are interpreted to be remnant subduction zones from the pre-break-up margin of Gondwana that have been reoriented as a result of the Cenozoic transcurrent deformation of the New Zealand region. A near surface gap in the southern part of this zone may be related to the proximity of the Hikurangi Plateau. Low upper-mantle velocities across southern South Island and northwest South Island and western North Island are inferred to document Gondwana continental lithosphere.

ACKNOWLEDGEMENTS

We acknowledge funding from the Government of New Zealand's Marsden Fund project GNS0901. FD acknowledges support of NZGSF. Monica Kohler provided the teleseismic tomography code, and data from the SAPSE array. Two insightful anonymous reviews and discussions with Martin Reyners and Phaedra Upton greatly improved this paper.

REFERENCES

Balance, P.F., 1993. The Paleo-Pacific, post-subduction, passive margin thermal relaxation sequence (Late Cretaceous-Paleogene) of the drifting New Zealand continent, in *South Pacific Sedimentary Basins, Sedimentary Basins of the World, 2,* pp. 93–110, ed. Balance, P.F., Elsevier.

Beaumont, C., Kamp, P., Hamilton, J. & Fullsack, P., 1996. The continental collision zone, South Island, New Zealand: comparison of geodynamical models and observations, *J. geophys. Res.,* **101**(B2), 3333–3359.

Beggs, J.M., Challis, G.A. & Cook, R.A., 1990. Basement geology of the Campbell plateau: implications for the Campbell Magnetic Anomaly system, *N. Zeal. J. Geol. Geophys.,* **3,** 401–404.

Bourguiguon, S., Stern, T. & Savage, M., 2007. Crust and mantle thickening beneath the southern portion of the Southern Alps, *N. Zeal., Geophys. J. Int.,* **168**(2), 681–690.

Cooper, R.A., 1979. Lower Paleozoic rocks of New Zealand, *J. R. Soc. N. Zeal.,* **9,** 29–84.

Cooper, R.A., 1989. Early Paleozoic terranes of New Zealand, *J. R. Soc.,* **19**(1) 73–112.

Darbyshire, F. & Lebedev, S., 2009. Rayleigh wave phase-velocity heterogeneity and multi-layered azimuthal anisotropy of the Superior Craton, Ontario, *Geophys. J. Int.,* **176,** 215–234.

Davey, F.J., 2010. Crustal seismic reflection profile across the alpine fault and coastal plain at Whataroa, South Island, *N. Zeal. J. Geol. Geophys.,* **53**(4), 359–368.

Davy, B., Hoernle, K. & Werner, R., 2008. Hikurangi Plateau: crustal structure, rifted formation, and Gondwana subduction history, *Geochem., Geophys., Geosyst.,* **9**(7), Q07004, doi:10.1029/2007GC001855.

Deschamp, F., Lebedev, S., Meier, T. & Trampert, J., 2008. Azimuthal anisotropy of Rayleigh-wave phase velocities in the East-central US, *Geophys. J. Int.,* **173,** 827–843.

Eberhart-Phillips, D. & Bannister, S.C., 2002. Three-dimensional crustal structure in the Southern Alps region of New Zealand from inversion of local earthquake and active source data, *J. geophys. Res. Solid Earth,* **107**(B10), doi:10.1029/2001JB000567.

Eberhart-Phillips, D. & Bannister, S.C., 2010. 3-D Imaging of Marlborough, New Zealand, subducted plate and strike slip fault systems, *Geophys. J. Int.,* **182,** 73–96.

Eberhart-Phillips, D. & Reyners, M.E., 2001. A complex, young subduction zone imaged by three-dimensional seismic velocity, Fiordland, New Zealand, *Geophys. J. Int.,* **146**(3), 731–746.

Eberhart-Phillips, D., Chadwick, M. & Bannister, S.C., 2008. Three-dimensional attenuation structure of the central and southern South Island, New Zealand, from local earthquakes, *J. geophys. Res.: Solid Earth,* **113,** B05308, doi:10.1029/2007JB0005359.

Eberhart-Phillips, D., Reyners, M., Bannister, S., Chadwick, M. & Ellis, S., 2010, Establishing a versatile 3-D seismic velocity model for New Zealand, *Seismol. Res. Lett.,* **81,** 992–1000.

Forsyth, P.J., Barrell, D.J.A. & Jongens, R., 2008. Geology of the Christchurch area: scale 1:250,000. Institute of Geological & Nuclear Sciences 1:250,000 geological map, 16, *GNS Science,* Lower Hutt, 67 p. + 1 folded map pp.

Fry, B., Deschamps, F., Kissling, E., Stehly, L. & Giardini, D., 2010. Layered azimuthal anisotropy of Rayleigh wave phase velocities in the European Alpine lithosphere inferred from ambient noise, *Earth planet. Sci. Lett.,* **297**(1/2), 95–102.

Gerbault, M., Davey, F. & Henrys, S., 2002. Three-dimensional lateral crustal thickening in the continental oblique collision: an example from the Southern Alps, New Zealand, *Geophys. J. Int.,* **150,** 770–779.

Godfrey, N.J., Davey, F., Stern, T.A. & Okaya, D., 2001. Crustal structure and thermal anomalies of the Dunedin Region, South Island, New Zealand, *J. geophys. Res., B, Solid Earth Planets,* **106**(12), 30 835–30 848.

Houseman, G.A. & Molnar, P., 1997. Gravitational (Rayleigh-Taylor) instability of a layer with non- linear viscosity and convective thinning of continental lithosphere, *Geophys. J. Int.,* **128,** 125–150.

Houseman, G.A., McKenzie, D.P. & Molnar, P., 1981. Convective instability of a thickened boundary layer and its relevance for the thermal evolution of continental convergent belts, *J. geophys. Res.,* **86,** 6115–6132.

Kamp, P.J.J., 1986. The mid-Cenozoic Challenger rift system of western New Zealand and its implications for the age of Alpine Fault inception, *Geol. Soc. Am. Bull.,* **97.3,** 255–281.

Kohler, M.D. & Eberhart-Phillips, D., 2002. Three-dimensional lithospheric structure below the New Zealand Southern Alps, *J. geophys. Res.,* **107**(B10), 2225, doi:10.1029/2001JB000182.

Meier, T., Dietrich, K., Stockert, B. & Harjes, H.-P., 2004. One-dimensional models of shear wave velocity for the eastern Mediterranean obtained from the inversion of Rayleigh wave phase velocities and tectonic implications, *Geophys. J. Int.,* **156**(1), 45–58.

Melhuish, A., Holbrook, W.S., Davey, F., Okaya, D.A. & Stern, T., 2005. Crustal and upper mantle seismic structure of the Australian Plate, South Island, New Zealand, *Tectonophysics,* **395,** 113–135.

Molnar, P. *et al.*, 1999. Continuous deformation versus faulting through the continental lithosphere of New Zealand, *Science,* **286,** 516–519.

Mortimer, N., 2004. New Zealand's geological foundations, *Gondwana Res.,* **7**(1), 261–272.

Munker, C. & Crawford, A.J., 2000. Cambrian arc evolution along the SE Gondwana active margin: a synthesis from Tasmania-New Zealand-Australia-Antarctica correlations, *Tectonics,* **19**(3), 415–432.

Nathan, S., Anderson, H.J., Cook, R.J., Herzer, R.H., Hoskins, R.H., Raine, J.I. & Smale, D., 1986. Cretaceous and Cenozoic sedimentary basins of the West Coast region, South Island, New Zealand, New Zealand Geological Survey basin studies 1, New Zealand Geological Survey, Lower Hutt.

Petersen, T., Gledhill, K., Chadwick, M., Gale, N.H. & Ristau, J., 2011. The New Zealand National Seismograph Network, *Seismol. Res. Lett.,* **82,** 9–20.

Reyners, M., Eberhart-Phillips, D. & Bannister, S., 2011. Tracking repeated subduction of the Hikurangi Plateau beneath New Zealand, *Earth planet. Sci. Lett.,* **311,** 165–171.

Scherwath, M., Stern, T., Davey, F., Okaya, D., Holbrook, W.S., Davies, R. & Kleffmann, S., 2003. Lithospheric structure across oblique continental collision in New Zealand from wide-angle P wave modeling, *J. geophys. Res., B, Solid Earth Planets,* **108**(B12), doi:10.1029/2002JB002286.

Scherwath, M., Stern, T., Davey, F. & Davies, R., 2006. Three-dimensional lithospheric deformation and gravity anomalies associated with oblique continental collision in South Island, New Zealand, *Geophys. J. Int.,* **167,** 906–916.

Smith, E.G.C. & Davey, F.J., 1984. Joint hypocentre determination of intermediate depth earthquakes in Fiordland, New Zealand, *Tectonophysics,* **104,** 127–144.

Spasojevic, S. & Clayton, R.W., 2008. Crustal structure and apparent tectonic underplating from receiver function analysis in South Island, New Zealand, *J. geophys. Res.,* **113,** B04307, doi:10.1029/2007JB005166.

Stehly, L., Fry, B., Campillo, M., Shapiro, N.M., Guilbert, J., Boschi, L. & Giardini, D. 2009. Tomography of the Alpine region from observations of seismic ambient noise, *Geophys. J. Int.,* **178**(1), doi:10.1111/j.1365-246X.2009.04132.x.

Stern, T., Molnar, P., Okaya, D. & Eberhart-Phillips, D., 2000. Teleseismic P wave delays and modes of shortening the mantle lithosphere beneath South Island, New Zealand, *J. geophys. Res.,* **105,** 21 615–21 631.

Suggate, P.R., Stevens, G.R. & Te Punga, M.T., eds, 1978. *The Geology of New Zealand,* 2 vols, N.Z. Government Printer.

Sutherland, R., 1999. Cenozoic bending of New Zealand basement terranes and Alpine Fault displacement: a brief review, *N. Zeal. J. Geol. Geophys.,* **42,** 295–301.

Sutherland, R., Davey, F. & Beavan, J., 2000. Plate boundary deformation in South Island, New Zealand, is related to inherited lithospheric structure, *Earth planet. Sci. Lett.,* **177,** 141–151.

Van Avendonk, H.J.A., Holbrook, W.S., Okaya, D., Austin, J.K., Davey, F. & Stern, T., 2004. Continental crust under compression: a seismic refraction study of SIGHT Transect I, South Island, New Zealand. *J. geophys. Res., B, Solid Earth Planets,* **109**(B6), doi:10.1029/2003JB002790.

Wodzicki, A., 1974. Geology of the pre-Cenozoic basement of the Taranaki-Cook Strait-Westland area, New Zealand, based on recent drillhole data, *N. Zeal. J. Geol. Geophys.,* **17,** 747–757.

Wood, R.A., 1991. Structure and stratigraphy of the western Challenger Plateau, *N. Zeal. J. Geol. Geophys.,* **34,** 1–9.

SUPPORTING INFORMATION

Additional Supporting Information may be found in the online version of this article:

Figure S1. Block hit counts showing data density for teleseismic rays used in the inversions for *Vp* (top panel) and *Vs* (bottom panel).
Figure S2. Synthetic test model with various 4 per cent high and 4 per cent low features, created using a finer grid than the teleseismic tomography was solved on.
Figure S3. Inversion results for the synthetic test data using 1-D initial model. Masking shows areas with insufficient data to constrain model velocities. Labels show cross-sections in Fig. S4.
Figure S4. Cross-sections through synthetic model presented in Fig. S2. Note, recovered anomalies are presented in d*Vp*.
Figure S5. Depth slices from the final 3-D *Vp* model based on the 1-D initial model shown at depth intervals of 40 km between 60 and 260 km depth. Solutions are obtained by averaging six inversions with different block linkages. Plots are masked where less than 20 rays traversed the blocks (http://gji.oxfordjournals.org/lookup/suppl/doi:10.1093/gji/ggt271/-/DC1)

Please note: Oxford University Press is not responsible for the content or functionality of any supporting materials supplied by the authors. Any queries (other than missing material) should be directed to the corresponding author for the article.